Superoxide Dismutase and Pseudocatalase Increase Tolerance to Hg(II) in *Thermus thermophilus* HB27 by Maintaining the Reduced Bacillithiol Pool

Javiera Norambuena,[a] Thomas E. Hanson,[b,c,d] Tamar Barkay,[a] Jeffrey M. Boyd[a]

[a]Department of Biochemistry and Microbiology, Rutgers, the State University of New Jersey, New Brunswick, New Jersey, USA
[b]School of Marine Science and Policy, University of Delaware, Newark, Delaware, USA
[c]Delaware Biotechnology Institute, Newark, Delaware, USA
[d]Department of Biological Sciences, University of Delaware, Newark, Delaware, USA

ABSTRACT Mercury (Hg) is a widely distributed, toxic heavy metal with no known cellular role. Mercury toxicity has been linked to the production of reactive oxygen species (ROS), but Hg does not directly perform redox chemistry with oxygen. How exposure to the ionic form, Hg(II), generates ROS is unknown. Exposure of *Thermus thermophilus* to Hg(II) triggered ROS accumulation and increased transcription and activity of superoxide dismutase (Sod) and pseudocatalase (Pcat); however, Hg(II) inactivated Sod and Pcat. Strains lacking Sod or Pcat had increased oxidized bacillithiol (BSH) levels and were more sensitive to Hg(II) than the wild type. The ΔbshA Δsod and ΔbshA Δpcat double mutant strains were as sensitive to Hg(II) as the ΔbshA strain that lacks bacillithiol, suggesting that the increased sensitivity to Hg(II) in the Δsod and Δpcat mutant strains is due to a decrease of reduced BSH. Treatment of *T. thermophilus* with Hg(II) decreased aconitase activity and increased the intracellular concentration of free Fe, and these phenotypes were exacerbated in Δsod and Δpcat mutant strains. Treatment with Hg(II) also increased DNA damage. We conclude that sequestration of the redox buffering thiol BSH by Hg(II), in conjunction with direct inactivation of ROS-scavenging enzymes, impairs the ability of *T. thermophilus* to effectively metabolize ROS generated as a normal consequence of growth in aerobic environments.

IMPORTANCE *Thermus thermophilus* is a deep-branching thermophilic aerobe. It is a member of the *Deinococcus-Thermus* phylum that, together with the *Aquificae*, constitute the earliest branching aerobic bacterial lineages; therefore, this organism serves as a model for early diverged bacteria (R. K. Hartmann, J. Wolters, B. Kröger, S. Schultze, et al., Syst Appl Microbiol 11:243–249, 1989, https://doi.org/10.1016/S0723-2020(89)80020-7) whose natural heated habitat may contain mercury of geological origins (G. G. Geesey, T. Barkay, and S. King, Sci Total Environ 569-570:321–331, 2016, https://doi.org/10.1016/j.scitotenv.2016.06.080). *T. thermophilus* likely arose shortly after the oxidation of the biosphere 2.4 billion years ago. Studying *T. thermophilus* physiology provides clues about the origin and evolution of mechanisms for mercury and oxidative stress responses, the latter being critical for the survival and function of all extant aerobes.

KEYWORDS *Thermus thermophilus*, bacillithiol, iron, mercury, pseudocatalase, reactive oxygen species, superoxide dismutase, thermophile

All aerobes face oxidative stress, which occurs when the balance between prooxidants and antioxidants is tipped toward prooxidants. Reactive oxygen species (ROS) are prooxidants that are produced by reduction of dioxygen. This can happen

intracellularly through the interaction of dioxygen with reduced flavin prosthetic groups (1). The transfer of one or two electrons to dioxygen produces superoxide ($O_2{}^-$) and hydrogen peroxide (H_2O_2), respectively (2). A three-electron transfer catalyzed by redox-active divalent transition metals, such as copper and iron (Fe) via Fenton and Haber-Weiss reactions, can produce hydroxyl radicals ($^\bullet OH$). These radicals are short-lived and rapidly react with multiple cellular constituents, including DNA (2).

Mercury (Hg) does not perform redox chemistry under biological conditions, but in animal models, Hg(II) exposure results in oxidative stress (3–7). Increased ROS upon Hg(II) exposure is thought to result from the depletion of cellular redox buffers (3, 6, 8) and/or the inhibition of the electron transport chain, allowing electrons to accumulate on flavoproteins (4, 6, 9). In bacteria, Hg(II) triggered the release of Fe(II) from solvent-exposed iron sulfur (Fe-S) clusters (10). Oxidation of solvent-accessible 4Fe-4S clusters by superoxide or H_2O_2 also results in Fe(II) release (11, 12). An increased pool of nonchelated or "free" cytosolic Fe(II) can accelerate Fenton chemistry (13).

Metabolic subsystems have evolved to detoxify Hg(II). Resistance to Hg(II) is encoded by the mercury resistance operon (mer), which is widely distributed over the bacterial and archaeal kingdoms (14). The gene composition of this operon varies among organisms, but all mer operons encode the mercuric reductase (MerA), which reduces Hg(II) to elemental mercury. Elemental Hg is volatile and diffuses out of the cell. Many mer operons also encode components involved in Hg(II) sequestration and/or transport and the Hg(II)-responsive transcriptional regulator of the operon, MerR (14). Deeply branching microbes have simple mer operons (15); the *Thermus thermophilus* operon is composed of *merA*, *merR*, and *oah2*. The latter encodes a homolog of *O*-acetyl-homocysteine sulfhydrylase, an enzyme normally involved in methionine biosynthesis and recycling (16, 17).

Our knowledge of the mer system comes from studies with the most derived taxa, including *Escherichia coli*, *Pseudomonas*, and *Bacillus*. *T. thermophilus* is a deep-branching thermophilic organism that responds differently to Hg(II) exposure than *E. coli* does (17). It possesses a different set of enzymes to detoxify ROS and uses bacillithiol (BSH) as the primary low-molecular-weight (LMW) thiol (17). *T. thermophilus* accumulates high concentrations of intracellular sulfides (324.1 ± 88.4 nmol/g [dry weight]) (17). Mercury has a high affinity for cellular thiols (18, 19), and exposure to 3 μM Hg(II) completely depleted free BSH pools in *T. thermophilus* (17). Interestingly, the cellular concentration of BSH is predicted to be an order of magnitude higher than the concentration of Hg(II) that depleted the reduced BSH pool (presented herein and in reference 17), suggesting that sequestration of BSH by Hg(II) is depleting only a portion of the BSH pool. These findings have led us to ask what happens to the rest of the BSH upon Hg(II) challenge. The disturbance of thiol-containing redox buffers, which play critical roles in ROS detoxification and oxidized protein repair, can lead to ROS accumulation (20). There is not a clearly established connection between Hg(II) and ROS in microbes, and even less is known about physiologically diverse microbes like *T. thermophilus* that utilize alternative redox buffers such as BSH.

We tested the overarching hypothesis that exposure of *T. thermophilus* to Hg(II) increases ROS accumulation because of decreased availability of reduced BSH. We demonstrate that Hg(II) exposure results in ROS accumulation. This is, in part, the result of Hg(II)-dependent inactivation of the ROS-metabolizing enzymes superoxide dismutase (Sod) and pseudocatalase (Pcat). Strains lacking ROS metabolizing enzymes contain decreased levels of reduced BSH and display increased sensitivity to Hg(II). Hg(II) exposure also inactivated aconitase, which requires a solvent-accessible Fe-S cluster, and increased free cytosolic Fe pools. This effect likely promotes ROS generation via Fenton chemistry, which we monitored by measuring DNA damage. Taken together, these findings confirm that an enzymatic capacity to detoxify ROS is important for the maintenance of a reduced intracellular thiol pool, which is necessary to mitigate Hg(II) toxicity in *T. thermophilus*.

RESULTS

Mercury exposure results in ROS accumulation and inactivates ROS-scavenging enzymes. We tested the hypothesis that Hg(II) exposure would increase ROS accumulation in *T. thermophilus*. After exposure to Hg(II), total intracellular ROS levels were qualitatively assessed with the fluorescent probe 2′,7′-dichlorodihydrofluorescein diacetate (H_2DCFDA). Exposure to 4 or 8 μM Hg(II) for 60 min resulted in a significant increase in DCFDA-based fluorescence, suggesting increased ROS accumulation (Fig. 1A).

The genome of *T. thermophilus* encodes one manganese-dependent superoxide dismutase (Sod) to detoxify superoxide. It does not possess catalase, but instead, it encodes a nonheme catalase, or pseudocatalase (Pcat), that utilizes an active site manganese to metabolize H_2O_2 (21). It also possesses two types of peroxiredoxins: osmotically inducible protein (OsmC) and bacterioferritin comigratory protein (Bcp). These are members of the thiol peroxidase family, which catalyze the reduction of hydroperoxides (22, 23). The genome also encodes a thioredoxin-related protein, thiol:disulfide interchange protein (TlpA), which is involved in oxidative stress responses (24).

We tested the hypothesis that Hg(II) exposure increases the transcription of genes involved in ROS detoxification. Exposure of *T. thermophilus* to 1 μM Hg(II) increased transcript levels of *sod*, *pcat*, *osmC*, and *tlpA* (Fig. 1B). This induction was noted after 7.5 min (not shown) and sustained for at least 30 min after Hg(II) exposure (Fig. 1B). Only *bcp* transcript levels were not significantly changed. The strongest induction was observed after 15 min of Hg(II) exposure. The greatest induction was noted for *pcat*, which was induced 107 $\pm$ 23-fold.

We next examined whether the increased transcription of *sod* and *pcat* would correlate with increased enzyme activity. Cells were exposed to Hg(II) for 30 min, and then H_2O_2 and superoxide (SOD)-scavenging activities were measured in cell-free lysates. Hg(II) exposure significantly increased H_2O_2 consumption by approximately twofold. A Δ*pcat* mutant strain lost >90% of the H_2O_2 consumption activity, suggesting that Pcat functions in H_2O_2 metabolism (Fig. 1C). Superoxide consumption appeared to increase relative to the unexposed control, but it was not statistically significant ($P = 0.249$) (Fig. 1C). A Δ*sod* strain displayed eightfold-lower superoxide-scavenging activity than the Hg(II)-unexposed parent, correlating superoxide consumption with the presence of Sod.

Comparing the transcript levels and enzymatic activities revealed a significant disconnect. Hg(II) exposure resulted in greatly increased *sod* and *pcat* transcript levels, without a commensurate increase in Sod and Pcat activities. We tested the hypothesis that Hg(II) exposure was detrimental to Sod and Pcat activities. We used *T. thermophilus* cell-free lysates generated from cells that had not been exposed to Hg(II). Incubation of the cell-free lysate with 100 μM Hg(II) resulted in a 70% decrease in Pcat activity (see Fig. S1C in the supplemental material). We were not able to conduct traditionally described SOD assays because xanthine oxidase was inhibited by Hg(II); therefore, we measured Sod and Pcat activities by zymography. When lysates were directly exposed to Hg(II), the activities of both Sod and Pcat were decreased (Fig. 1D and F). Gel-localized activities were verified using the Δ*sod* and Δ*pcat* strains (Fig. 1E and G). The Δ*sod* and Δ*pcat* strains were more sensitive to paraquat and H_2O_2, respectively (Fig. S1).

We examined whether Hg(II) affects Pcat and Sod *in vivo*. To this end, we stopped protein synthesis and incubated cells with 1 or 5 μM Hg(II) and without Hg(II) before H_2O_2 and superoxide consumption was monitored in cell-free lysates. In the absence of Hg(II), Pcat and Sod activities were approximately 50% after 30-min exposure to chloramphenicol (533 $\pm$ 26 and 3.9 $\pm$ 0.3 U/mg protein, respectively). Exposure to 5 μM Hg(II) further decreased consumption of superoxide by 25% (to 2.9 $\pm$ 0.3 U/mg) and consumption of H_2O_2 by 15% (to 453 $\pm$ 15 U/mg) compared to the cells treated with chloramphenicol only (Fig. 1H). Incubation with 1 μM Hg(II) did not result in a significant decrease in SOD or Pcat activities (not shown). These findings demonstrate that Hg(II) exposure resulted in ROS accumulation and increased activities of Pcat and Sod
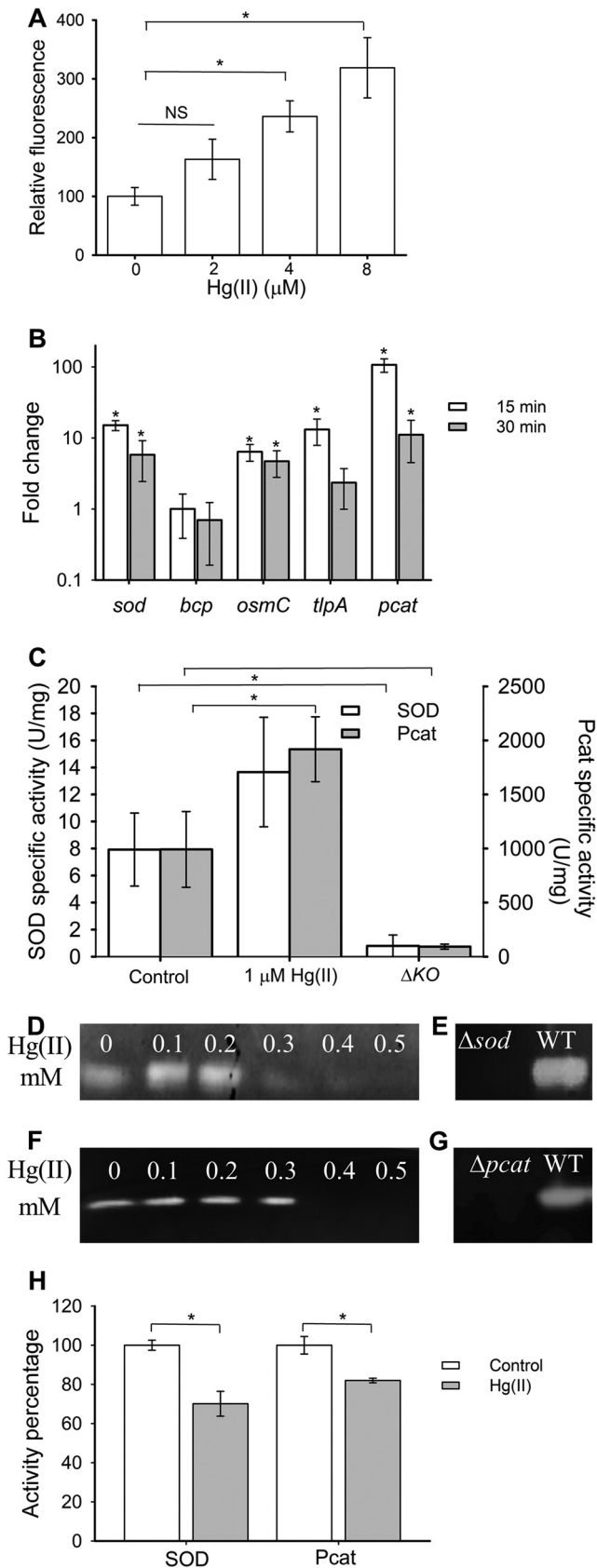
FIG 1 Mercury exposure induces ROS, increases Sod and Pcat expression, and inhibits SOD and Pcat activities. (A) Cultures of *T. thermophilus* (WT) were exposed to various concentrations of Hg(II) for 60 min
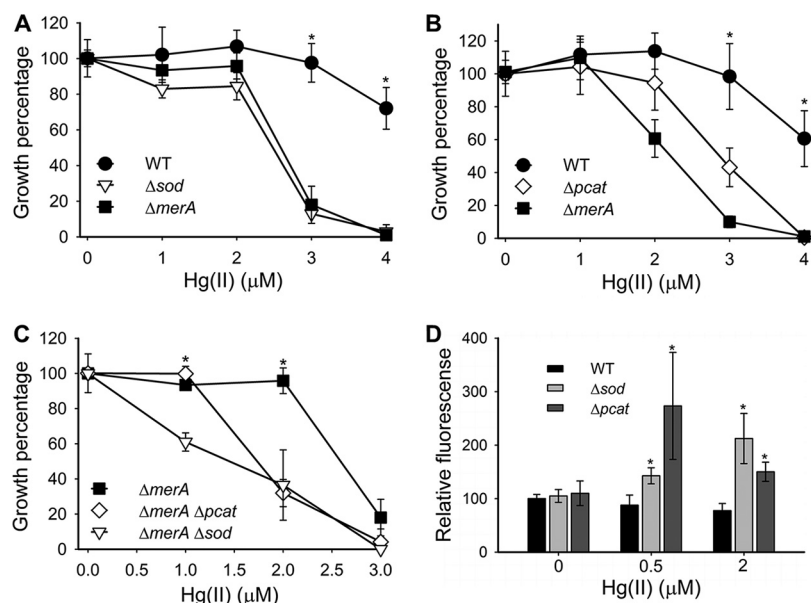
FIG 2 *T. thermophilus* strains lacking superoxide- or H_2O_2-scavenging activities are more sensitive to Hg(II) and have increased ROS levels upon Hg(II) exposure. The optical densities of cultures were determined after 21 h (A and C) or 18 h (B) of growth. Growth in the unexposed control was considered 100% growth. (D) Cultures were grown, and one-half of each culture was exposed to Hg(II) for 60 min before ROS were quantified using DCFDA. The fluorescence obtained for the unexposed WT strain was considered 100% fluorescence. Each point represents the average from three independent cultures, and standard deviations are shown. Student's *t* tests were performed, and an asterisk indicates a *P* of ≤0.05.

in vivo. However, the strong transcriptional induction of *pcat* and *sod* translated into only modest increases in Sod and Pcat activities. This could be, in part, the result of Hg(II) inhibition of the holoenzyme or of enzyme maturation.

Strains lacking superoxide- or H_2O_2-scavenging activities are more sensitive to Hg(II). We tested the hypothesis that Sod and Pcat have roles in mitigating Hg(II) toxicity. Compared to the parent strain (WT), *T. thermophilus* Δ*sod* and Δ*pcat* mutants had increased sensitivity to Hg(II) with 50% inhibitory concentrations (IC_{50}) of 2.5 μM and 3 μM, respectively (Fig. 2A and B). The WT IC_{50} for Hg(II) was 4.5 μM. The Δ*sod* strain was as sensitive to Hg(II) as the Δ*merA* strain. Genetic complementation of the Δ*sod* (Fig. S2A and C) and Δ*pcat* (Fig. S2B and D) strains verified that the lack of Sod or Pcat was responsible for the observed phenotypes.

We tested the hypothesis that the roles of Sod or Pcat in mitigating Hg(II) toxicity were independent of the function of MerA. We compared the Hg(II) sensitivities of the Δ*merA* Δ*sod* and Δ*merA* Δ*pcat* double mutants to that of the Δ*merA* mutant. The double mutant strains were more sensitive to Hg(II) than the Δ*merA* strain (Fig. 2C), suggesting

FIG 1 Legend (Continued)

before total ROS was measured using H_2DCFDA. (B) Induction of superoxide dismutase (*sod*), bacterio-ferritin comigratory protein (*bcp*), organic hydroperoxide reductase (*osmC*), thiol peroxidase (*tlpA*), and pseudocatalase (*pcat*) transcription was measured in the WT strain after 15 or 30 min of exposure to 1 μM Hg(II). (C) WT cells were exposed to 0 or 1 μM Hg(II) for 30 min and superoxide (white) and H_2O_2 (gray) consumption was monitored. Each activity was compared to the activity of the respective Δ*sod* or Δ*pcat* mutant strain (indicated as ΔKO in the figure) not exposed to Hg(II). (D to G) Crude protein extracts of the WT strain were incubated with different Hg(II) concentrations. Qualitative zymograms were revealed for SOD activity (D and E) or Pcat activity (F and G). Cell extracts of the WT and Δ*sod* strains (E) or WT and Δ*pcat* strains (G) are also shown. (H) WT cells were exposed to 150 μg/ml of chloramphenicol and incubated for 30 min with 0 (white) or 5 μM Hg(II) (gray); superoxide (SOD) and H_2O_2 (Pcat) consumption were monitored and activity percentages (relative to the unexposed strain [control]) are shown. For panels A, B, and C, each point represents the average from at least three independent experiments and standard deviations (error bars) are shown. For panel H, three replicate experiments are shown. Student's *t* tests were performed on the data in panels A and C, and an asterisk indicates a *P* of ≤0.05. A Mann-Whitney rank sum test was performed on the data in panel B, and an asterisk indicates a *P* of ≤0.05. NS, not significant.
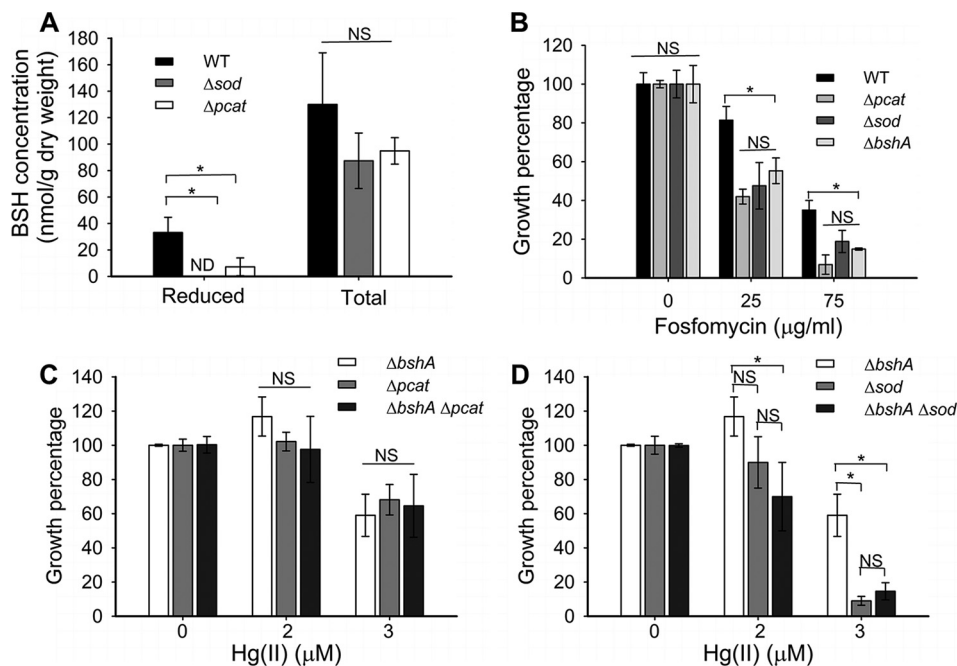
FIG 3 *T. thermophilus* strains lacking Sod or Pcat have decreased levels of reduced BSH pools. (A) Cultures were grown to an OD_{600} of 0.3 and exposed to 10 mM DTT or not exposed to DTT for 30 min before LMW thiols were quantified with mBrB. DTT-treated cells were used to measure total BSH. (B) Final culture optical densities were recorded after 20 h of growth in cultures exposed to various concentration of fosfomycin. (C and D) Effect of Hg(II) on cell growth was evaluated after 20 h of growth in the Δ*pcat*, Δ*bshA*, and Δ*pcat* Δ*bshA* strains (C) and in the Δ*sod*, Δ*bshA*, and Δ*sod* Δ*bshA* strains (D). Unexposed controls were considered 100% growth. Each point represents the average from three independent cultures, and standard deviations are shown. Student's *t* tests were performed on the data, and an asterisk indicates a *P* of ≤0.05. NS, not significant; ND, no signal detected.

that the roles of Sod, Pcat, and MerA in Hg(II) resistance are independent and complementary.

We next tested the corollary hypothesis that ROS accumulation would occur at lower Hg(II) concentrations in the Δ*sod* and Δ*pcat* strains compared to the WT strain. We were unable to detect ROS accumulation in the Δ*sod* and Δ*pcat* strains in the absence of Hg(II) (Fig. 2D). ROS accumulation was noted in the Δ*sod* and Δ*pcat* strains upon exposure to 0.5 and 2 μM Hg(II), whereas no change in ROS levels were noted in the WT strain. These results led us to conclude that Sod and Pcat mitigate Hg(II) toxicity by controlling ROS accumulation.

T. thermophilus strains lacking Sod or Pcat contain smaller reduced BSH pools. We tested the hypothesis that BSH functions in metabolizing ROS or the by-products of ROS damage. We quantified the reduced BSH pools in the Δ*sod* and Δ*pcat* strains by monobromobimane derivatization and HPLC, which quantifies free BSH pools. Free BSH was not detected in the Δ*sod* mutant (Fig. 3A), and the Δ*pcat* strain had 80% less free BSH than the WT strain (7.2 ± 6.7 versus 33.2 ± 10.2 nmol g⁻¹ [dry weight] for the WT) (Fig. 3A). Importantly, all strains had approximately the same intracellular concentration of total (reduced plus oxidized) BSH (Fig. 3A), strongly suggesting that the lack of free BSH is due to its oxidation in the mutant strains or defective recycling of bacillithiol disulfide (BSSB) back to BSH. The same HPLC traces did not display a significant difference in intracellular sulfide concentrations between the WT, Δ*sod*, and Δ*pcat* strains, but these peaks were quite broad, making it difficult to quantify accurately (data not shown).

Reduced BSH is required to detoxify the antibiotic fosfomycin (25) and mitigate oxidative stress (26). The Δ*sod* and Δ*pcat* strains were more sensitive to fosfomycin than the WT and had fosfomycin sensitivities similar to that of the Δ*bshA* strain (Fig. 3B), which cannot synthesize BSH (17). Compared to the WT strain, the Δ*bshA* strain showed
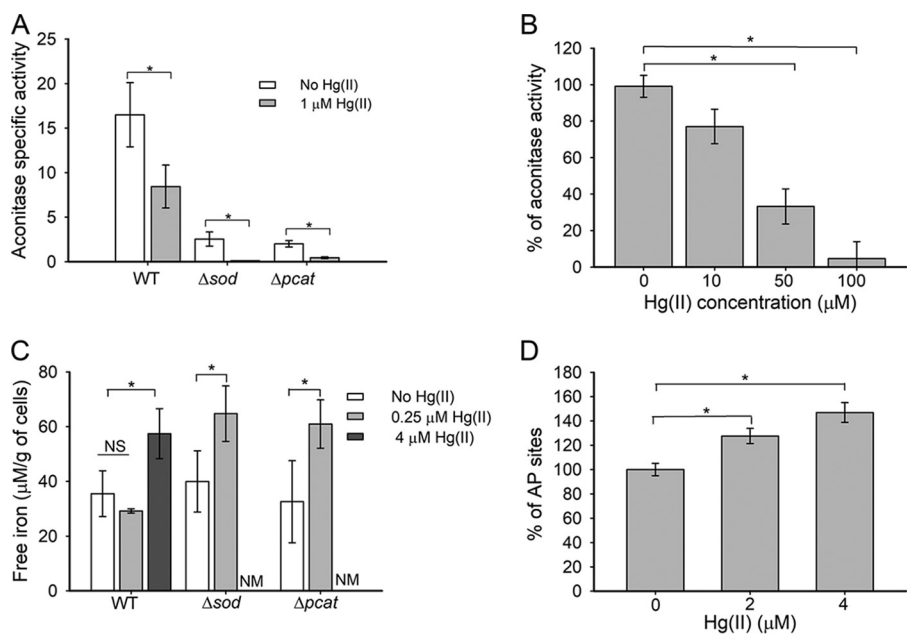
FIG 4 Hg(II) stress results in aconitase inactivation, increased intracellular free iron, and DNA damage. (A) Aconitase activity was monitored in cell-free lysates after whole cells had been exposed to 1 μM Hg(II) or not exposed to Hg(II) for 30 min. (B) Cell-free lysates from the WT strain were exposed to 0 to 100 μM Hg(II) before aconitase activity was determined. (C) The concentration of free Fe was quantified after exposure to 0.25 μM Hg(II) or to 4 μM Hg(II) for 30 min. Cell weight is reported as wet weight. (D) DNA damage was determined by quantifying the number of apurinic/apyrimidinic sites (AP sites) in the WT strain [cells unexposed to Hg(II) had an average of 8.38 $\pm$ 0.77 AP sites per 100,000 bp of DNA]. Each point represents the average from at least three independent cultures, and standard deviations are shown. Where shown, Student's t tests were conducted on the data, and an asterisk indicates a P of $\leq$0.05. NS, not significant; NM, not measured.

increased sensitivity to H_2O_2 and paraquat; however, the $\Delta bshA$ strain was less sensitive to the toxicants than the Δsod and $\Delta pcat$ strains (Fig. S1).

ROS-scavenging deficient strains were constructed in the $\Delta bshA$ background to test whether Hg(II) sensitivity in the $\Delta pcat$ and Δsod strains was exacerbated by a complete lack of BSH (17). The Hg(II) sensitivity phenotypes corresponding to the $\Delta bshA$ and $\Delta pcat$ mutations were not additive (Fig. 3C), but the Δsod strain was more sensitive to 3 μM Hg(II) than the $\Delta bshA$ strain was (Fig. 3D). These results suggested that Sod has a role in preventing Hg(II) toxicity in addition to its role in preventing the oxidation of the BSH pool, while the Hg(II) sensitivity of the $\Delta pcat$ strain appears to result from a lack of reduced BSH.

Hg(II) exposure results in decreased aconitase (AcnA) activity, increased free cytosolic Fe, and DNA damage. BSH plays a fundamental role in Hg(II) resistance in *T. thermophilus*, and exposure to 3 μM Hg(II) completely depleted free BSH pools (17). The Δsod and $\Delta pcat$ strains had decreased concentrations of reduced BSH (Fig. 3A), suggesting that there may be more free Hg(II) in the cytoplasms of the Δsod and $\Delta pcat$ strains when challenged with Hg(II). Prior work in *E. coli* found that Hg(II) inactivated fumarase, which requires a solvent-accessible Fe-S cluster for catalysis (10). When *T. thermophilus* was exposed to 1 μM Hg(II) for 30 min, AcnA activity decreased to 50% of the unexposed control (Fig. 4A). The nonchallenged $\Delta pcat$ and Δsod strains had 12 and 16% of the activity of the WT strain, respectively (Fig. 4A). Upon exposure to Hg(II), AcnA activity was reduced a further 30-fold in the Δsod strain and 4.5-fold in the $\Delta pcat$ strain (Fig. 4A). We next examined whether Hg(II) inactivated *T. thermophilus* AcnA *in vitro*. To this end, we added Hg(II) to anaerobic cell-free lysates prior to measuring AcnA activity. AcnA activity decreased as a function of Hg(II) added and was nearly unde-tected after exposure to 100 μM Hg(II) (Fig. 4B).

We next tested the hypothesis that Hg(II) exposure would increase the size of the cytosolic free Fe pool. *T. thermophilus* was exposed to 4 μM Hg(II) or not exposed to
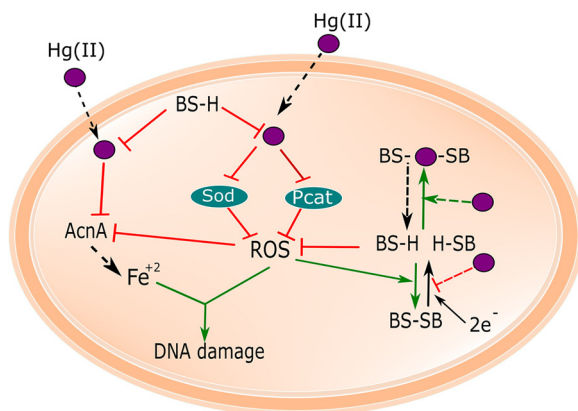
FIG 5 Working model for ROS generation by Hg(II). Exposure of *T. thermophilus* to Hg(II) (purple) results in the inactivation of two ROS-detoxifying enzymes (Sod and Pcat) and ROS accumulation. Hg(II) decreases bioavailable BSH, which is necessary to prevent Hg(II) intoxication and ROS accumulation. The presence of Sod and Pcat are necessary to maintain reduced BSH pools, as well as to metabolize superoxide and H_2O_2, respectively. Hg(II) accumulation inactivates enzymes, such as aconitase, with solvent-accessible Fe-S clusters and increases intracellular free Fe. The free Fe^{2+} participates in Fenton chemistry producing hydroxyl radicals, which damage DNA. Systems inhibited are shown in red, and systems favored upon Hg(II) toxicity are shown in green.

Hg(II) for 30 min, and intracellular free Fe was quantified using electron paramagnetic resonance (EPR) spectroscopy (19, 27). Exposure significantly increased the pool of free Fe by 1.7-fold (Fig. 4C). When the WT, Δ*sod*, and Δ*pcat* strains were exposed to 0.25 μM Hg(II), the WT free Fe pool was unaltered, while it was significantly increased, 1.8-fold, in the Δ*sod* and Δ*pcat* strains; however, at 4 μM Hg(II), the free Fe pool was elevated in the WT strain (Fig. 4C). Thus, treatment with a lower concentration of Hg(II) was capable of disrupting the Fe homeostasis in the Δ*sod* and Δ*pcat* strains compared to the WT. These strains had similar free Fe levels when cultured in the absence of Hg(II) (Fig. 4C).

Free Fe(II) can catalyze Fenton chemistry to produce HO• (2) that can damage DNA (28) by producing apurinic/apyrimidinic (AP) sites (29, 30). We hypothesized that Hg(II) exposure would result in increased DNA damage. After exposure to either 2 or 4 μM Hg(II), there was a significant increase in AP sites (Fig. 4D). Repair of AP sites requires base excision repair, which in *T. thermophilus* depends on the Nfo endonuclease IV (31). A *T. thermophilus* Δ*nfo* mutant was more sensitive to Hg(II) than the WT strain (Fig. S3).

Taken together, these data are consistent with a model wherein Hg(II) exposure decreases the activities of enzymes requiring solvent-exposed Fe-S clusters and increases intracellular free Fe. The increase in free Fe likely contributes to increased hydroxyl radicals resulting in increased DNA damage.

DISCUSSION

The mechanisms by which metals exert toxicity are not fully understood. These phenomena have largely been examined in model organisms, and relatively few studies have been conducted in physiologically or phylogenetically diverse organisms. In this study, we examined the effect of Hg(II) exposure on a deeply branching thermophilic bacterium to expand our knowledge of Hg(II) toxicity and tolerance in phylogenetically and physiologically diverse microbes.

Data presented herein, and from our previous study (17), have led to a working model for how Hg(II) exposure affects *T. thermophilus* (Fig. 5). In our model, increased titers of cytosolic Hg(II) result in ROS accumulation, which also may be the result of Hg(II)-dependent inactivation of Sod and Pcat. Strains lacking Sod or Pcat have increased levels of oxidized BSH. Reduced BSH is necessary to buffer both cytosolic Hg(II) and ROS. In the absence of reduced BSH, Hg(II) accumulation inactivates enzymes, such as aconitase, with solvent-accessible Fe-S clusters and increases intracellular free Fe. The increased free Fe(II) participates in Fenton chemistry, resulting in an increase in

hydroxyl radicals causing DNA damage. Thus, exposure to Hg(II) results in oxidative stress even though Hg(II) is not a redox-active metal, and mutations that diminish cellular defenses against ROS indirectly increase Hg(II) sensitivity. It is also probable that BSH directly acts as a Hg(II) ligand (17, 32).

Oxidative stress among the prokaryotes has been mostly examined in *E. coli* with little attention to physiologically diverse microbes. *Thermus* spp. inhabit hot environments where heat lowers maximal oxygen saturation (4.53 mg/liter at 65°C) relative to saturation under conditions utilized to culture *E. coli* (6.73 mg/liter at 37°C) (33). When tested, *Thermus aquaticus* grew better under microaerophilic conditions compared to more aerated conditions, correlating with a decreased ability to detoxify ROS (34). These facts may also explain the presence of pseudocatalase rather than catalase (35). Relative to *E. coli*, *T. thermophilus* displays a distinct gene expression pattern upon Hg(II) exposure. In *T. thermophilus*, *sod*, *pcat*, *osmC*, and *tlpA* transcripts, but not *bcp*, were induced in response to Hg(II) (Fig. 1A). In *E. coli*, Hg(II) was found to induce the expression of *sodB* and the peroxiredoxin *ahpC*, but not *katG* and *katE* that encode catalases (36). The *E. coli sodA*, which is the *T. thermophilus sod* orthologue, was repressed by short-term Hg(II) exposure (36). We previously showed that *E. coli* and *T. thermophilus* differentially regulate the transcription of genes required for LMW-thiol synthesis upon Hg(II) exposure (17). Taken together, these findings highlight the fact that these two bacteria, one deep branching and the other highly derived, differ in their responses to Hg(II). The findings reported here, therefore, provide a foundation for future studies to decipher how microbial systems have evolved in response to the combined toxic effects of metals and oxygen.

The amount of BSH in *T. thermophilus* cells appears to be lower than the concentration of glutathione typically found in Gram-negative bacteria. Assuming that *T. thermophilus* cells have the same volume and dry weight as *E. coli* cells, the cytosolic concentration of BSH would be ~40 μM under the growth conditions utilized. Previous work found the concentration of BSH in *Bacillus subtilis* and *Deinococcus radiodurans* to be ~200 μM (37). The concentration of glutathione in *E. coli* cells is ~5 mM (37). The lower concentration of BSH in *T. thermophilus* cells could constrain the ability to use BSH to buffer against ROS when Hg(II) accumulates in the cytosol. This could result in an increased reliance on alternative ROS-mitigating factors, such as Sod, to protect the cell.

BSH pools were decreased by incubation with Hg(II) (17) and in mutant strains lacking Pcat or Sod. We found that BSH functions to prevent ROS poisoning in *T. thermophilus* (see Fig. S1 in the supplemental material). The Δ*sod* and Δ*pcat* strains had lower levels of reduced BSH, but the same overall concentration of BSH (Fig. 3A), suggesting that ROS or a by-product of ROS metabolism results in increased BSH oxidation. A role for BSH as a buffer against ROS accumulation could explain why there was no detected difference in ROS titers in the Δ*sod*, Δ*pcat*, and WT strains in the absence of Hg(II). It is currently unknown which enzyme(s) is (are) responsible for reducing BSSB back to BSH in *T. thermophilus*. In yeast and protists, glutathione reductase is inhibited by Hg(II) (38, 39) and if *T. thermophilus* utilizes a similar enzyme to reduce BSSB, which is likely, it is possible that this enzyme is also inhibited by Hg(II), resulting in a decreased ability to recycle BSSB to BSH (Fig. 5). It was hypothesized that YpdA functions as a BSSB reductase in *B. subtilis* (40). The genome of *T. thermophilus* encodes a gene product that is 39% identical to YpdA (NCBI accession no. YP_144481). Future studies will be necessary to determine the effect of this gene product on BSSB recycling.

In some cyanobacteria, glutaredoxin reductase possesses a mercuric reductase activity (41), and it is thus conceivable that MerA in *Thermus* may serve as a BSSB reductase. This possibility is hard to evaluate with our current mechanistic understanding of MerA, which is largely based on studies with proteobacterial reductases (42, 43). MerA in *Thermus* is a core MerA, lacking the 70-amino-acid N terminus (NmerA) (44) that functions in delivering S-Hg-S to the redox active site of the enzyme (43) and thus must differ from the full-length proteobacterial variants in interaction with its substrates. We

also found that the reduced BSH pool in the Δ*merA* strain was similar to that of the WT (not shown).

We previously reported the high concentrations of sulfides in strain HB27 (324.1 ± 88.4 nmol/g [dry weight]) (17). The natural habitats for *Thermus* spp. are usually moderate- to high-temperature terrestrial springs with low sulfide and circumneutral to alkaline pH, suggesting a chemoorganotrophic metabolism (45, 46). However, genome sequences of several *Thermus* spp., including HB27, revealed presence of genes related to the SOX and PSR systems (47). These systems may specify mixotrophic growth with reduced sulfur as an energy source and anaerobic polysulfide respiration, respectively (48). We are not aware of reports demonstrating such metabolic capabilities in *Thermus*, and our findings in this paper and our previous paper (17) highlight the need for further research on this topic.

Hg(II) readily reacts with sulfide to form HgS, and evidence suggests that sulfide production could be a Hg(II) detoxification mechanism (49). We did not notice a significant decrease in the size of the sulfide pool upon challenge with Hg(II) (17); however, the small amount of Hg(II) added to *T. thermophilus* cultures relative to the size of the sulfide pool likely render it impossible to detect a decline in sulfide concentration upon Hg(II) binding. Hydrogen sulfide has been found to aid in the detoxification of ROS (50–52). In the future, we would like to decrease the size of the sulfide pool and examine the consequences on ROS metabolism and Hg(II) challenge.

Hg(II) inhibited Sod, Pcat, and AcnA *in vivo* and *in vitro*, but a higher concentration of Hg(II) was required to inhibit these enzymes *in vitro*. Moreover, the concentrations of Hg(II) necessary to inhibit SOD and Pcat *in vitro* were much higher than predicted to accumulate inside cells under the growth conditions utilized. Among the scenarios that could explain this discrepancy, the most plausible explanation might be the difference in available Hg(II) *in vivo* and *in vitro*. Mercury bioavailability is greatly affected by the presence of ligands (53–55). If cell lysis during preparation of crude cell extracts releases ligands that are compartmentalized within intact cells, these may greatly reduce Hg(II) bioavailability in *in vitro* assays. This is suggested by our laboratory's protocols for mercuric reductase assays whereby resting cells and crude extract activities are measured at 10 and 100 μM Hg(II) (56), respectively. The high concentrations of sulfide in strain HB27 (17), which are likely present as labile organic and inorganic persulfides and polysulfides (57), may greatly limit Hg(II) bioavailability in crude cell extracts. The precise nature of the intracellular sulfide pool in strain HB27 and how it interacts with metals and other stressors will be an important future avenue of investigation.

This study reports on the effects of Hg(II) on *T. thermophilus*, which belongs to one of the earliest aerobic bacterial lineages (68) inhabiting high mercury environments (69). We report that ROS detoxification is important for Hg(II) tolerance; therefore, in *T. thermophilus*, resistance to Hg(II) is achieved through both *mer*-based detoxification (16, 17) and the oxidative stress response. We previously suggested that the *mer* system evolved in response to the oxygenation of earth due to the increased availability of oxidized Hg species (44). It is likely that these same environmental changes led to the evolution of the oxidative stress response. While numerous reports have documented metal-induced oxidative stress (reviewed in references 8, 58, and 59), few examined how responses to this stress alleviate metal toxicity among prokaryotes. Our findings in *T. thermophilus* alert us to these hitherto little-studied aspects of metal homeostasis.

MATERIALS AND METHODS

Chemicals and bacterial growth conditions. *Thermus thermophilus* HB27 (WT) and its mutants were cultured at 65°C in 461 Castenholz TYE medium (complex medium [CM]) (16). When cultured in liquid medium, cells were grown in 3 ml of medium in 10-ml test tubes incubated perpendicularly and shaken at 200 rpm. Test tubes were used to grow cells for ROS analysis, RNA extraction, resistance assays, and AP site quantification. Flasks (2:3 gaseous headspace to liquid medium ratio) were used to grow cultures to generate cell extracts for enzyme assays, zymograms, thiol content determination, and for intracellular Fe concentration determination. Solid culture medium was supplemented with 1.5% (wt/vol) agar. Kanamycin (Kan) and hygromycin B were supplemented at 25 μg ml^{-1} and 40 μg ml^{-1}, respectively. Unless otherwise stated, overnight (ON) cultures of *T. thermophilus* were diluted in fresh medium to an optical density at 600 nm (OD$_{600}$) of 0.1 and further grown to OD$_{600}$ of ~0.3 before challenged with

toxicants (fosfomycin, paraquat, or $HgCl_2$). Mercury was used as $HgCl_2$ for all assays. Protein concentrations were determined using the Quick Start Bradford protein assay (Bio-Rad Laboratories Inc., Hercules, CA).

Mutant construction. The in-frame deletions for *sod* (WP_011172643.1) and *pcat* (WP_011174225.1) were performed as previously described (17). DNA primers used in this study are listed in Table S1 in the supplemental material. Gene replacements were confirmed by DNA sequencing. For genetic complementation, the 16S rRNA gene (*rrsB*; TT_C3024), was replaced with the complementing gene constructs by the method of Gregory and Dahlberg (60). All mutant strains used the native gene promoter to express resistance cassettes or genes.

Monitoring reactive oxygen species. The fluorophore 2',7'-dichlorodihydrofluorescein diacetate (H_2DCFDA) (61–63) was used for ROS monitoring. Cells were incubated for 60 min in the presence or absence of Hg(II). Cells from 1 ml of culture were pelleted, washed with phosphate-buffered saline (PBS), resuspended in 500 μl of 10 μM H_2DCFDA in PBS, and incubated for 30 min at 37°C. After incubation, cells were washed with PBS and lysed by sonication. Fluorescence was measured (Perkin Elmer HTS 7000 Plus Bio assay reader) at 485 nm as the excitation wavelength and 535 nm as the emission wavelength. Data were normalized to protein concentration.

RNA extraction, cDNA synthesis, and qPCR. For induction of gene expression, cells were exposed to 1 μM Hg(II) for 15 or 30 min. Three-milliliter aliquots were removed and mixed with RNA protect (Qiagen). RNA extraction and cDNA synthesis were performed as previously described (17). Transcripts were quantified by qPCR (iCycler iQ; Bio-Rad Laboratories Inc., Hercules, CA) as previously described (17). DNA primers and cycling temperatures used are listed in Table S2.

Enzymatic assays. Cultures (25 ml) were exposed to Hg(II) for 30 min, cells were pelleted and washed with PBS, and cell pellets were frozen until further use. Crude cell extracts were prepared as previously described (56). All enzyme assays were performed at 50°C. For exposure of crude cell lysates, Hg(II) was added at the indicated concentrations and incubated for 5 min before measuring enzymatic activity. The assay described by Oberley and Spitz (64) was used to determine SOD activity with 30 μg of crude extract. One unit was defined as the amount of enzyme needed to reduce the reference rate by 50% (64). Measurements were carried out with an AVIV 14 UV-VI spectrophotometer. Catalase activity was measured by the method of Beers and Seizer (65) with 0.6 mg of protein extract. One unit was defined as the amount of enzyme needed to degrade 1 μmol of H_2O_2 per min ($\varepsilon = 43.6 \ M^{-1} \ cm^{-1}$ for H_2O_2). For aconitase activity, cell lysis was performed under anaerobic conditions as described elsewhere (66) with 20 μg of protein extract. One unit was defined as the amount of enzyme needed to degrade one μmol of DL-isocitrate per s ($\varepsilon = 3.6 \ mM^{-1} \ cm^{-1}$ for *cis*-aconitate). To determine the *in vivo* Hg(II)-dependent inhibition of H_2O_2 and superoxide consumptions, protein synthesis was stopped by adding 150 μg chloramphenicol/ml to cells grown to an OD_{600} of ~0.3, before 5 μM Hg(II) was added. Cells were incubated for 30 min before harvesting as described above. Catalase and aconitase activities were measured with a UVmini-1240 spectrophotometer (Shimadzu Corporation, Kyoto, Japan).

Resistance assays. Overnight cultures were diluted to an OD_{600} of 0.1 in fresh CM, and various concentrations of toxicant (fosfomycin, paraquat, or $HgCl_2$) were added to individual samples at different concentration ranges. Resistance was assessed as the percentage of growth observed at the indicated times relative to the control that was not exposed to the toxicant (100% growth). Soft agar assays were used to assess H_2O_2 sensitivity. Cells were grown as for liquid assays, and 40 μl of the culture was added to 4 ml of CM soft agar (0.8% [wt/vol]) and then poured over a 25-mm petri dish with CM agar. Ten microliters of 10 mM H_2O_2 was added to the center of the plate. The halo of growth inhibition was measured after 24-h incubation.

Zymograms. SOD and catalase in-gel activities were performed as described elsewhere (67). For SOD and Pcat activities, 25 μg and 50 μg, respectively, of cell lysates were loaded on the gels. Cell lysates were prepared as described above for enzymatic assays.

Thiol concentration determination. Extraction and quantification of low-molecular-weight thiols were performed as previously described (17). Briefly cells were resuspended in D-mix (acetonitrile, HEPES, EDTA, and mBrB) and incubated for 15 min at 60°C in the dark. Free thiols are complexed with mBrB before the reaction was stopped with methanesulfonic acid. Samples were centrifuged, and cell debris was separated from the soluble thiols before quantifying LMW thiols by HPLC. Cell debris was dried to determine the dry weight of cell material derived from each sample. For total BSH determinations, cells were exposed to 10 mM DTT for 30 min prior to thiol extraction.

Intracellular iron quantification. The intracellular iron quantification assay was performed by the method of LaVoie et al. (19). Cultures (100 ml) were exposed to Hg(II) for 30 min. Cells were pelleted by centrifugation, resuspended in 5 ml of PBS with 10 mM diethylene triamine pentaacetic acid (DTPA) and 20 mM deferoxamine mesylate salt (DF), shaken at 37°C for 15 min at 180 rpm, and pelleted at 4°C. Cells were washed once with ice-cold 20 mM Tris-HCl (pH 7.4), resuspended in the same buffer with 15% (vol/vol) glycerol, and stored at −80°C. For EPR analysis, cell suspensions were thawed on ice, and 200-μl aliquots were dispensed into 4-mm OD quartz EPR tubes and frozen in liquid nitrogen. Continuous-wave (CW) EPR experiments were performed with an X-band Bruker EPR spectrometer (Elexsys580) equipped with an Oxford helium flow cryostat (ESR900) and an Oxford temperature controller (ITC503). EPR parameters used in our experiments were as follows: microwave frequency, 9.474 GHz; microwave power, 20 mW; modulation amplitude, 2 mT; and sample temperature, 25°K. The Fe(III)/DF concentration of each sample was determined by comparing the peak-to-trough height of EPR signal at $g = 4.3$ against the standard sample with a known Fe(III)/DF concentration (50 μM $FeCl_3$ and 20 mM DF in 20 mM Tris-HCl at pH 7.4 with 15% [vol/vol] glycerol).

Quantification of apurinic or apyrimidinic (AP) sites. Cells were exposed to Hg(II) for 60 min. Three-milliliter aliquots of cultures were pelleted and washed with PBS prior to DNA extraction using QIAamp DNA kit (Qiagen). AP sites were quantified using the Oxiselect oxidative DNA damage quantification kit (Cell Biolabs).

Statistical analysis. One-way ANOVA followed by a Dunnet test analysis was performed for multiple group comparison to a control. For two group comparisons (controls versus treatment), Student's t tests were performed.

Data availability. All data will be provided upon request.

SUPPLEMENTAL MATERIAL

Supplemental material for this article may be found at https://doi.org/10.1128/mBio .00183-19.

FIG S1, TIF file, 4.6 MB.
FIG S2, TIF file, 5 MB.
FIG S3, TIF file, 2 MB.
TABLE S1, DOCX file, 0.01 MB.
TABLE S2, DOCX file, 0.01 MB.

ACKNOWLEDGMENTS

REFERENCES

1. Messner KR, Imlay JA. 2002. Mechanism of superoxide and hydrogen peroxide formation by fumarate reductase, succinate dehydrogenase, and aspartate oxidase. J Biol Chem 277:42563–42571. https://doi.org/10.1074/jbc.M204958200.
2. Imlay JA. 2003. Pathways of oxidative damage. Annu Rev Microbiol 57:395–418. https://doi.org/10.1146/annurev.micro.57.030502.090938.
3. Valko M, Morris H, Cronin MTD. 2005. Metals, toxicity and oxidative stress. Curr Med Chem 12:1161–1208. https://doi.org/10.2174/0929867053764635.
4. Miller DM, Lund BO, Woods JS. 1991. Reactivity of Hg(II) with superoxide: evidence for the catalytic dismutation of superoxide by Hg(II). J Biochem Toxicol 6:293–298. https://doi.org/10.1002/jbt.2570060409.
5. Ariza ME, Bijur GN, Williams MV. 1998. Lead and mercury mutagenesis: role of H$_2$O$_2$, superoxide dismutase, and xanthine oxidase. Environ Mol Mutagen 31:352–361. https://doi.org/10.1002/(SICI)1098-2280(1998)31:4<352::AID-EM8>3.0.CO;2-K.
6. Lund BO, Miller DM, Woods JS. 1991. Mercury-induced H$_2$O$_2$ production and lipid peroxidation in vitro in rat kidney mitochondria. Biochem Pharmacol 42(Suppl):S181–S187. https://doi.org/10.1016/0006-2952(91)90408-W.
7. Ariza ME, Williams MV. 1999. Lead and mercury mutagenesis: type of mutation dependent upon metal concentration. J Biochem Mol Toxicol 13:107–112. https://doi.org/10.1002/(SICI)1099-0461(1999)13:2<107::AID-JBT6>3.0.CO;2-0.
8. Ercal N, Gurer-Orhan H, Aykin-Burns N. 2001. Toxic metals and oxidative stress part I: mechanisms involved in metal-induced oxidative damage. Curr Top Med Chem 1:529–539. https://doi.org/10.2174/1568026013394831.
9. Nath KA, Croatt AJ, Likely S, Behrens TW, Warden D. 1996. Renal oxidant injury and oxidant response induced by mercury. Kidney Int 50:1032–1043. https://doi.org/10.1038/ki.1996.406.
10. Xu FF, Imlay JA. 2012. Silver(I), mercury(II), cadmium(II), and zinc(II) target exposed enzymic iron-sulfur clusters when they toxify Escherichia coli. Appl Environ Microbiol 78:3614–3621. https://doi.org/10.1128/AEM.07368-11.
11. Keyer K, Imlay JA. 1996. Superoxide accelerates DNA damage by elevating free-iron levels. Proc Natl Acad Sci U S A 93:13635–13640. https://doi.org/10.1073/pnas.93.24.13635.
12. Jang S, Imlay JA. 2007. Micromolar intracellular hydrogen peroxide disrupts metabolism by damaging iron-sulfur enzymes. J Biol Chem 282:929–937. https://doi.org/10.1074/jbc.M607646200.
13. Imlay JA, Chin SM, Linn S. 1988. Toxic DNA damage by hydrogen peroxide through the Fenton reaction in vivo and in vitro. Science 240:640–642. https://doi.org/10.1126/science.2834821.
14. Barkay T, Miller SM, Summers AO. 2003. Bacterial mercury resistance from atoms to ecosystems. FEMS Microbiol Rev 27:355. https://doi.org/10.1016/S0168-6445(03)00046-9.
15. Boyd ES, Barkay T. 2012. The mercury resistance operon: from an origin in a geothermal environment to an efficient detoxification machine. Front Microbiol 3:349. https://doi.org/10.3389/fmicb.2012.00349.
16. Wang Y, Freedman Z, Lu-Irving P, Kaletsky R, Barkay T. 2009. An initial characterization of the mercury resistance (mer) system of the thermophilic bacterium Thermus thermophilus HB27. FEMS Microbiol Ecol 67:118. https://doi.org/10.1111/j.1574-6941.2008.00603.x.
17. Norambuena J, Wang Y, Hanson T, Boyd JM, Barkay T. 2018. Low-molecular-weight thiols and thioredoxins are important players in Hg(II) resistance in Thermus thermophilus HB27. Appl Environ Microbiol 84:e01931-17. https://doi.org/10.1128/AEM.01931-17.
18. Oram PD, Fang X, Fernando Q, Letkeman P, Letkeman D. 1996. The formation constants of mercury(II)–glutathione complexes. Chem Res Toxicol 9:709–712. https://doi.org/10.1021/tx9501896.
19. LaVoie SP, Mapolelo DT, Cowart DM, Polacco BJ, Johnson MK, Scott RA, Miller SM, Summers AO. 2015. Organic and inorganic mercurials have distinct effects on cellular thiols, metal homeostasis, and Fe-binding proteins in Escherichia coli. J Biol Inorg Chem 20:1239–1251. https://doi.org/10.1007/s00775-015-1303-1.
20. Murphy MP. 2009. How mitochondria produce reactive oxygen species. Biochem J 417:1–13. https://doi.org/10.1042/BJ20081386.
21. Hidalgo A, Betancor L, Moreno R, Zafra O, Cava F, Fernandez-Lafuente R, Guisan JM, Berenguer J. 2004. Thermus thermophilus as a cell factory for the production of a thermophilic Mn-dependent catalase which fails to be synthesized in an active form in Escherichia coli. Appl Environ Microbiol 70:3839–3844. https://doi.org/10.1128/AEM.70.7.3839-3844.2004.
22. Clarke DJ, Ortega XP, Mackay CL, Valvano MA, Govan JR, Campopiano DJ, Langridge-Smith P, Brown AR. 2010. Subdivision of the bacteriofer-

ritin comigratory protein family of bacterial peroxiredoxins based on catalytic activity. Biochemistry 49:1319–1330. https://doi.org/10.1021/bi901703m.

23. Flohe L, Toppo S, Cozza G, Ursini F. 2011. A comparison of thiol peroxidase mechanisms. Antioxid Redox Signal 15:763–780. https://doi.org/10.1089/ars.2010.3397.

24. Achard ME, Hamilton AJ, Dankowski T, Heras B, Schembri MS, Edwards JL, Jennings MP, McEwan AG. 2009. A periplasmic thioredoxin-like protein plays a role in defense against oxidative stress in *Neisseria gonorrhoeae*. Infect Immun 77:4934–4939. https://doi.org/10.1128/IAI.00714-09.

25. Gaballa A, Newton GL, Antelmann H, Parsonage D, Upton H, Rawat M, Claiborne A, Fahey RC, Helmann JD. 2010. Biosynthesis and functions of bacillithiol, a major low-molecular-weight thiol in bacilli. Proc Natl Acad Sci U S A 107:6482–6486. https://doi.org/10.1073/pnas.1000928107.

26. Chi BK, Gronau K, Mäder U, Hessling B, Becher D, Antelmann H. 2011. S-Bacillithiolation protects against hypochlorite stress in *Bacillus subtilis* as revealed by transcriptomics and redox proteomics. Mol Cell Proteomics 10:M111.009506. https://doi.org/10.1074/mcp.M111.009506.

27. Woodmansee AN, Imlay JA. 2002. Quantitation of intracellular free iron by electron paramagnetic resonance spectroscopy. Methods Enzymol 349:3–9. https://doi.org/10.1016/S0076-6879(02)49316-0.

28. de Mello Filho AC, Meneghini R. 1985. Protection of mammalian cells by o-phenanthroline from lethal and DNA-damaging effects produced by active oxygen species. Biochim Biophys Acta 847:82–89. https://doi.org/10.1016/0167-4889(85)90156-9.

29. Kanno S, Iwai S, Takao M, Yasui A. 1999. Repair of apurinic/apyrimidinic sites by UV damage endonuclease; a repair protein for UV and oxidative damage. Nucleic Acids Res 27:3096–3103. https://doi.org/10.1093/nar/27.15.3096.

30. Kidane D, Murphy DL, Sweasy JB. 2014. Accumulation of abasic sites induces genomic instability in normal human gastric epithelial cells during *Helicobacter pylori* infection. Oncogenesis 3:e128. https://doi.org/10.1038/oncsis.2014.42.

31. Morita R, Nakane S, Shimada A, Inoue M, Iino H, Wakamatsu T, Fukui K, Nakagawa N, Masui R, Kuramitsu S. 2010. Molecular mechanisms of the whole DNA repair system: a comparison of bacterial and eukaryotic systems. J Nucleic Acids 2010:179594. https://doi.org/10.4061/2010/179594.

32. Rosario-Cruz Z, Boyd JM. 2016. Physiological roles of bacillithiol in intracellular metal processing. Curr Genet 62:59–65. https://doi.org/10.1007/s00294-015-0511-0.

33. Mortimer CH. 1981. The oxygen content of air-saturated fresh waters over ranges of temperature and atmospheric pressure of limnological interest. Int Ver Theor Angew 22:1–23. https://doi.org/10.1080/05384680.1981.11904000.

34. Allgood GS, Perry JJ. 1986. Characterization of a manganese-containing catalase from the obligate thermophile *Thermoleophilum album*. J Bacteriol 168:563–567. https://doi.org/10.1128/jb.168.2.563-567.1986.

35. Whittaker MM, Barynin VV, Antonyuk SV, Whittaker JW. 1999. The oxidized (3,3) state of manganese catalase. Comparison of enzymes from *Thermus thermophilus* and *Lactobacillus plantarum*. Biochemistry 38:9126–9136. https://doi.org/10.1021/bi990499d.

36. Onnis-Hayden A, Weng H, He M, Hansen S, Ilyin V, Lewis K, Guc AZ. 2009. Prokaryotic real-time gene expression profiling for toxicity assessment. Environ Sci Technol 43:4574–4581. https://doi.org/10.1021/es803227z.

37. Newton GL, Rawat M, La Clair JJ, Jothivasan VK, Budiarto T, Hamilton CJ, Claiborne A, Helmann JD, Fahey RC. 2009. Bacillithiol is an antioxidant thiol produced in bacilli. Nat Chem Biol 5:625–627. https://doi.org/10.1038/nchembio.189.

38. Picaud T, Desbois A. 2006. Interaction of glutathione reductase with heavy metal: the binding of Hg(II) or Cd(II) to the reduced enzyme affects both the redox dithiol pair and the flavin. Biochemistry 45:15829–15837. https://doi.org/10.1021/bi061304m.

39. Shigeoka S, Onishi T, Nakano Y, Kitaoka S. 1987. Characterization and physiological function of glutathione reductase in *Euglena gracilis* z. Biochem J 242:511–515. https://doi.org/10.1042/bj2420511.

40. Helmann JD. 2011. Bacillithiol, a new player in bacterial redox homeostasis. Antioxid Redox Signal 15:123–133. https://doi.org/10.1089/ars.2010.3562.

41. Marteyn B, Sakr S, Farci S, Bedhomme M, Chardonnet S, Decottignies P, Lemaire SD, Cassier-Chauvat C, Chauvat F. 2013. The *Synechocystis* PCC6803 MerA-like enzyme operates in the reduction of both mercury

and uranium under the control of the glutaredoxin 1 enzyme. J Bacteriol 195:4138–4145. https://doi.org/10.1128/JB.00272-13.

42. Ledwidge R, Patel B, Dong A, Fiedler D, Falkowski M, Zelikova J, Summers AO, Pai EF, Miller SM. 2005. NmerA, the metal binding domain of mercuric ion reductase, removes Hg²⁺ from proteins, delivers it to the catalytic core, and protects cells under glutathione-depleted conditions. Biochemistry 44:11402–11416. https://doi.org/10.1021/bi050519d.

43. Lian P, Guo HB, Riccardi D, Dong A, Parks JM, Xu Q, Pai EF, Miller SM, Wei DQ, Smith JC, Guo H. 2014. X-ray structure of a Hg²⁺ complex of mercuric reductase (MerA) and quantum mechanical/molecular mechanical study of Hg²⁺ transfer between the C-terminal and buried catalytic site cysteine pairs. Biochemistry 53:7211–7222. https://doi.org/10.1021/bi500608u.

44. Barkay T, Kritee K, Boyd E, Geesey G. 2010. A thermophilic bacterial origin and subsequent constraints by redox, light and salinity on the evolution of the microbial mercuric reductase. Environ Microbiol 12:2904–2917. https://doi.org/10.1111/j.1462-2920.2010.02260.x.

45. Brock TD. 1981. Extreme thermophiles of the genera Thermus and Sulfolobus, p 978–984. *In* Starr MP, Stolp H, Trüper HG, Balows A, Schlegel HG (ed), The prokaryotes. Springer-Verlag, Berlin, Germany.

46. Kristjansson JK, Alfredsson GA. 1983. Distribution of *Thermus* spp. in Icelandic hot springs and a thermal gradient. Appl Environ Microbiol 45:1785–1789.

47. Murugapiran SK, Huntemann M, Wei C-L, Han J, Detter JC, Han C, Erkkila TH, Teshima H, Chen A, Kyrpides N, Mavrommatis K, Markowitz V, Szeto E, Ivanova N, Pagani I, Pati A, Goodwin L, Peters L, Pitluck S, Lam J, McDonald AI, Dodsworth JA, Woyke T, Hedlund BP. 2013. *Thermus oshimai* JL-2 and *T. thermophilus* JL-18 genome analysis illuminates pathways for carbon, nitrogen, and sulfur cycling. Stand Genomic Sci 7:449–468. https://doi.org/10.4056/sigs.3667269.

48. Jormakka M, Yokoyama K, Yano T, Tamakoshi M, Akimoto S, Shimamura T, Curmi P, Iwata S. 2008. Molecular mechanism of energy conservation in polysulfide respiration. Nat Struct Mol Biol 15:730–737. https://doi.org/10.1038/nsmb.1434.

49. Glendinning KJ, Macaskie LE, Brown NL. 2005. Mercury tolerance of thermophilic *Bacillus* sp. and *Ureibacillus* sp. Biotechnol Lett 27:1657–1662. https://doi.org/10.1007/s10529-005-2723-8.

50. Spassov SG, Donus R, Ihle PM, Engelstaedter H, Hoetzel A, Faller S. 2017. Hydrogen sulfide prevents formation of reactive oxygen species through PI3K/Akt signaling and limits ventilator-induced lung injury. Oxid Med Cell Longev 2017:3715037. https://doi.org/10.1155/2017/3715037.

51. Chang L, Geng B, Yu F, Zhao J, Jiang H, Du J, Tang C. 2008. Hydrogen sulfide inhibits myocardial injury induced by homocysteine in rats. Amino Acids 34:573–585. https://doi.org/10.1007/s00726-007-0011-8.

52. Geng B, Chang L, Pan C, Qi Y, Zhao J, Pang Y, Du J, Tang C. 2004. Endogenous hydrogen sulfide regulation of myocardial injury induced by isoproterenol. Biochem Biophys Res Commun 318:756–763. https://doi.org/10.1016/j.bbrc.2004.04.094.

53. Hsu-Kim H, Kucharzyk KH, Zhang T, Deshusses MA. 2013. Mechanisms regulating mercury bioavailability for methylating microorganisms in the aquatic environment: a critical review. Environ Sci Technol 47:2441–2456. https://doi.org/10.1021/es304370g.

54. Barkay T, Gillman M, Turner RR. 1997. Effects of dissolved organic carbon and salinity on bioavailability of mercury. Appl Environ Microbiol 63:4267–4271.

55. Farrell RE, Germida JJ, Huang PM. 1993. Effects of chemical speciation in growth media on the toxicity of mercury(II). Appl Environ Microbiol 59:1507–1514.

56. Vetriani C, Chew YS, Miller SM, Yagi J, Coombs J, Lutz RA, Barkay T. 2005. Mercury adaptation among bacteria from a deep-sea hydrothermal vent. Appl Environ Microbiol 71:220–226. https://doi.org/10.1128/AEM.71.1.220-226.2005.

57. Luebke JL, Shen J, Bruce KE, Kehl-Fie TE, Peng H, Skaar EP, Giedroc DP. 2014. The CsoR-like sulfurtransferase repressor (CstR) is a persulfide sensor in *Staphylococcus aureus*. Mol Microbiol 94:1343–1360. https://doi.org/10.1111/mmi.12835.

58. Nies DH. 1999. Microbial heavy-metal resistance. Appl Microbiol Biotechnol 51:730–750. https://doi.org/10.1007/s002530051457.

59. Hobman JL, Crossman LC. 2015. Bacterial antimicrobial metal ion resistance. J Med Microbiol 64:471–497. https://doi.org/10.1099/jmm.0.023036-0.

60. Gregory ST, Dahlberg AE. 2009. Genetic and structural analysis of base

substitutions in the central pseudoknot of *Thermus thermophilus* 16S ribosomal RNA. RNA 15:215–223. https://doi.org/10.1261/rna.1374809.

61. Wang H, Joseph JA. 1999. Quantifying cellular oxidative stress by dichlorofluorescein assay using microplate reader. Free Radic Biol Med 27:612–616. https://doi.org/10.1016/S0891-5849(99)00107-0.

62. Myhre O, Andersen JM, Aarnes H, Fonnum F. 2003. Evaluation of the probes 2',7'-dichlorofluorescin diacetate, luminol, and lucigenin as indicators of reactive species formation. Biochem Pharmacol 65:1575–1582. https://doi.org/10.1016/S0006-2952(03)00083-2.

63. Rosario-Cruz Z, Chahal HK, Mike LA, Skaar EP, Boyd JM. 2015. Bacillithiol has a role in Fe-S cluster biogenesis in *Staphylococcus aureus*. Mol Microbiol 98:218–242. https://doi.org/10.1111/mmi.13115.

64. Spitz DR, Oberley LW. 1989. An assay for superoxide dismutase activity in mammalian tissue homogenates. Anal Biochem 179:8–18. https://doi.org/10.1016/0003-2697(89)90192-9.

65. Beers RF, Jr, Sizer IW. 1952. A spectrophotometric method for measuring the breakdown of hydrogen peroxide by catalase. J Biol Chem 195:133–140.

66. Mashruwala AA, Boyd JM. 2017. The *Staphylococcus aureus* SrrAB regulatory system modulates hydrogen peroxide resistance factors, which imparts protection to aconitase during aerobic growth. PLoS One 12:e0170283. https://doi.org/10.1371/journal.pone.0170283.

67. Weydert CJ, Cullen JJ. 2010. Measurement of superoxide dismutase, catalase and glutathione peroxidase in cultured cells and tissue. Nat Protoc 5:51–66. https://doi.org/10.1038/nprot.2009.197.

68. Hartmann RK, Wolters J, Kröger B, Schultze S, Specht T, Erdmann VA. 1989. Does *Thermus* represent another deep eubacterial branching? Syst Appl Microbiol 11:243–249. https://doi.org/10.1016/S0723-2020(89)80020-7.

69. Geesey GG, Barkay T, King S. 2016. Microbes in mercury-enriched geothermal springs in western North America. Sci Total Environ 569-570:321–331. https://doi.org/10.1016/j.scitotenv.2016.06.080.